SiGe quantum wells implementation in Si based nanowires for solar cells applications

M. Safi, A. Aissat, H. Guesmi, Jean-Pierre Vilcot

SiGe quantum wells implementation in Si based nanowires for solar cells applications

M. Safi[a,*], A. Aissat[a,b,*], H. Guesmi[a], J. P. Vilcot[b]
[a]*Faculty of Technology, University of Blida1, Blida, Algeria*
[b]*Institute of Electronics, Microelectronics and Nanotechnology (IEMN), UMR CNRS 8520. University of Sciences and Technologies of Lille 1Avenue Poincare, 60069,59652 Villeneuve of Ascq, France*

This study focuses on modelling and optimizing a new Si nanowire solar cell containing a SiGe/Si quantum well. Quantum efficiency measurements show that the proposed structure has a higher energy absorption advantage and stronger than that of a solar cell based on a standard Si p-i-n nanowire. As a result, the insertion of 14 layers of SiGe/Si quantum well improved the short circuit current density and the efficiency by a factor of about 1.24 and 1.37, respectively. The best concentration and radius values obtained are x = 0.05 and r = 0.190 µm, respectively, with a strain of less than 1%.

(Received December 30, 2022; Accepted March 7, 2023)

Keywords: Nanowire, Quantum wells, Solar cells, Quantum efficiency

1. Introduction

During this last decade, the discovery of nanostructures has changed the world of research. This technology, which is a tool for system design and characterization, recognized the day at the speed of light thanks to its nanometric size, which happens to be the major point of its success. In order to exceed the Shockley Queisser efficiency limit of 30% [1], the development of new generation solar cells relies on nanostructures. These nanostructures are still in the process of development, which has made it possible to achieve high power conversion efficiency, with a relatively low cost compromise. The solar spectrum contains photons with energies ranging from about 0.5 to 3.5 eV. Photons with energies below the semiconductor bandgap are not absorbed. To reduce the losses of low energy photons, the researchers aim to develop structures that allow us to absorb the maximum photons of the solar spectrum, which led us to minimize the losses. Inside this concept, we have the nanostructure including Quantum Wells (QWs), Quantum Dots (QDs) and Nanowires (NWs) [2-5]. The main motivation has been the ability to customize the properties of materials at the nanoscale, through size and structure, in a way that is impossible at the macro scale. Key aspects being exploited are nanostructuring to enhance the absorption and conversion of photons across the solar spectrum to generate charge carriers. Nanometrics devices are designed to efficiently harvest the charge carriers for electrical energy generation. Areas of current research attention include nanoparticle multiexciton effects to create more than one electron–hole pair per absorbed photon [6, 7].

In this paper, we focus on nanowire thanks to their potential applications to solar energy harvesting. Recently, enormous amount of research effort was started towards finding new architectures that gives a high conversion efficiency. The present study uses Si material, whose structure is of diamond type belonging to column IV of the periodic table [7]. This material is known to be the most abundant chemical element on earth after oxygen, ideal for photovoltaic power generation [8]. Also, $Si_{1-x}Ge_x$ alloy, known for its interesting electronic and optical properties. It has become a favorable material for quantum wells, which was recently proven. Comparing a solar cell with 80 layers of SiGe quantum wells with a Si-based p-i-n solar cell, it was found that the short circuit current J_{cc} increases from 23.55 to 37.48 mA/cm^2 with a relative

* Corresponding author: sakre23@yahoo.fr
https://doi.org/10.15251/DJNB.2023.181.327

increase of 59.15% [9]. The latter plays a key role in improving the performance of Si-based microelectronic and optoelectronic devices [10].

For this purpose, we have proposed a new structure of p-i-n axial Si-Nanowires known for its structural performances as well as for its attractive physical properties, which has been proved recently [11]. This structure including SiGe quantum wells (NWQWs), was the subject of a previous report [12]. Silicon-based nanowires are also characterized by the emergence of new potential applications in several fields such as the elaboration of electronic components, photovoltaic devices, bio-chemical or mechanical sensors, in the medical field for imaging, and also for thermoelectrics [13,14]. In this study, the structural characteristics of a SiGe/Si quantum well solar cell is studied and optimized, with the aim of showing the effect of Germanium concentration and QW number on the important characteristics of a Si-Nanowire solar cell: current density voltage (J-V), power voltage (P-V) and quantum efficiency (QE).

2. Theoretical models

In this work we used the self-consistent coupled Schrödinger Poisson equations to model the effects of quantization in the quantum well and it is given on 1D for electrons and heavy holes respectively by:

$$\frac{-h^2}{2}\frac{\partial}{\partial Z}\left(\frac{1}{m_e^*}\frac{\partial \psi_i}{\partial Z}\right) + (U_c(z) - E_{ne})\psi_i \ = 0 \tag{1}$$

$$\frac{-h^2}{2}\frac{\partial}{\partial z}\left(\frac{1}{m_{hh}^*}\frac{\partial \psi_i}{\partial z}\right) + (U_v(z) - E_{nhh})\,\psi_i \ = 0 \tag{2}$$

where U_c and U_v are the conduction band and valence band edge respectively, m_e^* and m_{hh}^* are the effective mass of electrons and heavy holes respectively, ψ_i and E_{ne} are the wave function and energy level of the electrons (heavy holes) of the n subband. The lattice constant for $Si_{1-x}Ge_x$ structure is determinate by Vegard's law [15].

$$a_{SiGe}(x) = x.a_{Ge} + (1 - x).a_{Si} \tag{3}$$

The component of the strain is given by [15].

$$\varepsilon = \frac{a_{SiGe} - a_{Si}}{a_{Si}} \tag{4}$$

where a_{SiGe} and a_{Si} are the lattice constants for the SiGe and Si layers, respectively. The fitted empirical bandgap energy for strained Si1-xGex is given as fellow [15].

$$E_g^{SiGe} = 1.17 - 0.94.x + 0.34.x^2 \tag{5}$$

In order to optimize the layers thickness of the structure we studied the critical thickness (h_c). This thickness allows us to avoid the dislocation of the structure. So, we used several models. The value of the critical thickness is given by the following equation [16-18].

$$h_c = \frac{b}{a_{epit}} \times \frac{1}{8\pi(1+\gamma)} \times \ln\left(\frac{h_c}{b} + 1\right) \tag{6}$$

$$\varepsilon = \left(\frac{b\cos\lambda}{2\,h_c}\right)\left(\left(\frac{1-\frac{v}{4}}{4\pi(1+\gamma)cos^2\lambda}\right)\left(ln\frac{h_c}{b}\right) + 1\right) \tag{7}$$

where a_{epit} is the lattice parameter of the relaxed layer, b is the intensity of the Burgers vector, λ is the angle between the Burgers vector and the direction in the interface, normal to the dislocation line, Υ is the Poisson's coefficient given by: $\Upsilon = \frac{C_{12}}{c_{11}+c_{12}}$ with C_{ij} are the elastic coefficients.

The Drift-Diffusion model is used to calculate the current density of electrons and holes, and is given by the continuity equations [19].

$$\frac{\partial p}{\partial t} = G - U - \frac{1}{q}\left(\vec{\nabla}.J_p\right) \tag{8}$$

$$\frac{\partial n}{\partial t} = G - U + \frac{1}{q}\left(\vec{\nabla}.J_n\right) \tag{9}$$

where, p and n are the hole and electron densities respectively, and J_p and J_n are the hole and electron current densities, respectively. G and U are the photo-generation rate and the Shockley–Read–Hall (SRH) recombination rate, respectively.

The following equations are used to determine the current of hole and electron in the case of the drift-diffusion model [20].

$$J_p = q\mu_h p\vec{\nabla}E + qD_h\vec{\nabla}p \tag{10}$$

$$J_n = -q\mu_e n\vec{\nabla}E + qD_e\vec{\nabla}n \tag{11}$$

where E is the electric field, D_h (D_e) is the thermal diffusions of the holes(electrons) and μ_h(μ_e) is the holes(electrons) mobility.

The Poisson equation is given by the following equations where we assume no dependence on θ due to the circular symmetry of the electrostatic potential [20]:

$$\frac{\partial^2 V}{\partial z^2} + \frac{1}{r}.\frac{\partial V}{\partial r} + \frac{\partial^2 V}{\partial r^2} = \frac{-\rho(z,r)}{\varepsilon} \tag{12}$$

where ε is the permittivity, r is cylinder radius and V is the electrostatic potential.

In the case of quantum well systems the current continuity equations are given as fellow:

$$\frac{dn_{qw}}{dt} = G_{qw} - U_{qw} + \frac{n_b}{\tau_{cn}} - \frac{n_{qw}}{\tau_{en}} = 0 \tag{13}$$

$$\frac{dp_{qw}}{dt} = G_{qw} - U_{qw} + \frac{p_b}{\tau_{cp}} - \frac{p_{qw}}{\tau_{ep}} = 0 \tag{14}$$

where G_{qw} is the Photo-Generation rate, U_{qw} is the SRH recombination rate of quantum well, τ_{en}(τ_{ep}) is the electron(hole) escape times, τ_{cn}(τ_{cp}) is the electron(hole) capture time, p_b(n_b) is the hole(electron) density of the barrier and p_{qw}(n_{qw}) is the hole(electron) density of quantum well.

The external quantum efficiency (EQE) of the photogenerated carriers in n/p regions and in the intrinsic region which contains the QW layers, is calculated by [21].

$$EQE(\lambda) = \left(1 - R(\lambda)\right).\exp - (\alpha_p d_p + \alpha_n d_n + \alpha_{int} d) \tag{15}$$

where,

$R(\lambda)$ is the surface reflectivity, and it is set it to 0.1;
α_n and α_p are the absorption coefficients of the n and p regions;
d_n and d_p are their corresponding thicknesses, respectively;
α_{int} is the total intrinsic region absorption, it is given by Eq. 16.

$$\alpha_{int} d = \alpha_b d_b + \alpha_{Qw} d_{Qw} \tag{16}$$

where d is the total thickness of the intrinsic region, α_b and α_{QW} are the absorption coefficients of the barrier and quantum well materials. The absorption coefficient of the absorber layer is calculated via the model [22-25].

$$\alpha(\hbar\omega) = \frac{\pi e^2}{n_r c \varepsilon_0 m_0^2 \omega} \sum_i P^2 \delta(E_{tr} - \hbar\omega)\,(f_v - f_c) \tag{17}$$

$$P^2 = \frac{m_0^2}{3}\left[1 - \frac{m_e^*}{m_0}\right]\frac{E_g(E_g+\Delta_0)}{m_e^*\left(E_g+\frac{2}{3}\Delta_{so}\right)} \tag{18}$$

$$E_{tr} = E_g + E_{ne} + E_{nhh} \tag{19}$$

where E_{tr} is the transition energy, E_{ne} is the quantization energy levels of the electrons, E_{nhh} is the quantization energy levels of the heavy holes, E_g is the bandgap energy, f_c and f_v are the Fermi Dirac function for electrons and holes, m_0 is the electron mass in vacuum, m_e^* is the effective electron mass, $\hbar\omega$ is the photon energy, e is the charge electron, c is the light speed, n_r is the refractive index and Δ_{so} is the spin-orbit-splitting energy.

3. Results and discussion

In this work, the solar spectrum AM1.5 is chosen under a temperature of 300K, as a standard condition. All the binary parameters used in this simulation are presented in Table 1.

Table 1. Binary parameters used in this simulation

Material	Si	Ge
Lattice constant a (Å)	5.431	5.658
Bandgap E_g (eV)	1.12	0.66
Dielectric constant (ε_r)	11.7	16.2
Electron Affinity (eV)	4.05	4.0
Effective density of states in the conduction band N_c (cm^{-3})	$3.2\times10^{+19}$	$1.0\times10^{+19}$
Effective density of states in the valence band N_v (cm^{-3})	$1.8\times10^{+19}$	$5.0\times10^{+18}$
Electron mobility ($cm^2\ V^{-1}\ s^{-1}$)	1400	3900
Hole mobility ($cm^2\ V^{-1}\ s^{-1}$)	450	1900

First of all, we started the simulation by varying the germanium concentration in order to choose the appropriate value, which will allow us to obtain the best performances of the cell using a fixed number of quantum wells (4 QWs). Then we are interested in the variation of the QWs numbers inserted in the intrinsic region of the Si p-i-n nanowires in order to study the influence of their integration on different characteristics of the cell. We have also strengthened this study by determining the EQE and the absorption coefficients. In addition, the variation of the radius and temperature are also discussed; the results of the simulation are provided below.

Figure 1 shows the solar cell structure based on a single silicon nanowire (Fig 1.a), and a nanowire with $Si_{1-x}Ge_x$ quantum well insertion in Figure 1(b) The nanowire has a radius of 190 nm and a variable length depending on the number of inserted quantum wells, this latter has a length of 3 nm followed by a barrier with 8 nm in length. Figure 1(c) shows the confinement effect, i.e. the phenomenon of energy states created by the wells insertion. This phenomenon can lead to the absorption of low energy photons, because the integrated wells cause the formation of sub-layers, allowing low energy electrons to pass through, resulting in better absorption.

Figure 2 shows the variation of the bandgap energy and strain as a function of germanium concentration. The bandgap energy is compared with other measured bandgap energies for validation [26,27]. As shown in the figure, when the germanium concentration increases, on the one hand the bandgap energy decreases and on the other hand the strain increases. For example, the bandgap energy decreases from 1.17 to 0.58 eV and the strain increases from 0.02% to 4%,

when the germanium concentration increases from 0% to 100%. Moreover, we note that there is only one strain (compressive strain) whatever the germanium concentration. For this, we will vary the concentration of germanium in the interval {0 1}, in order to determine the best value of germanium concentration that gives the best performance. Figure. 3 shows the variation of the critical thickness depending on the germanium concentration, the two curve in black and red represent our results using Eq (6 and 7), the other curves (blue, green and magenta) represent the experimental results calculated by [28-30], respectively.

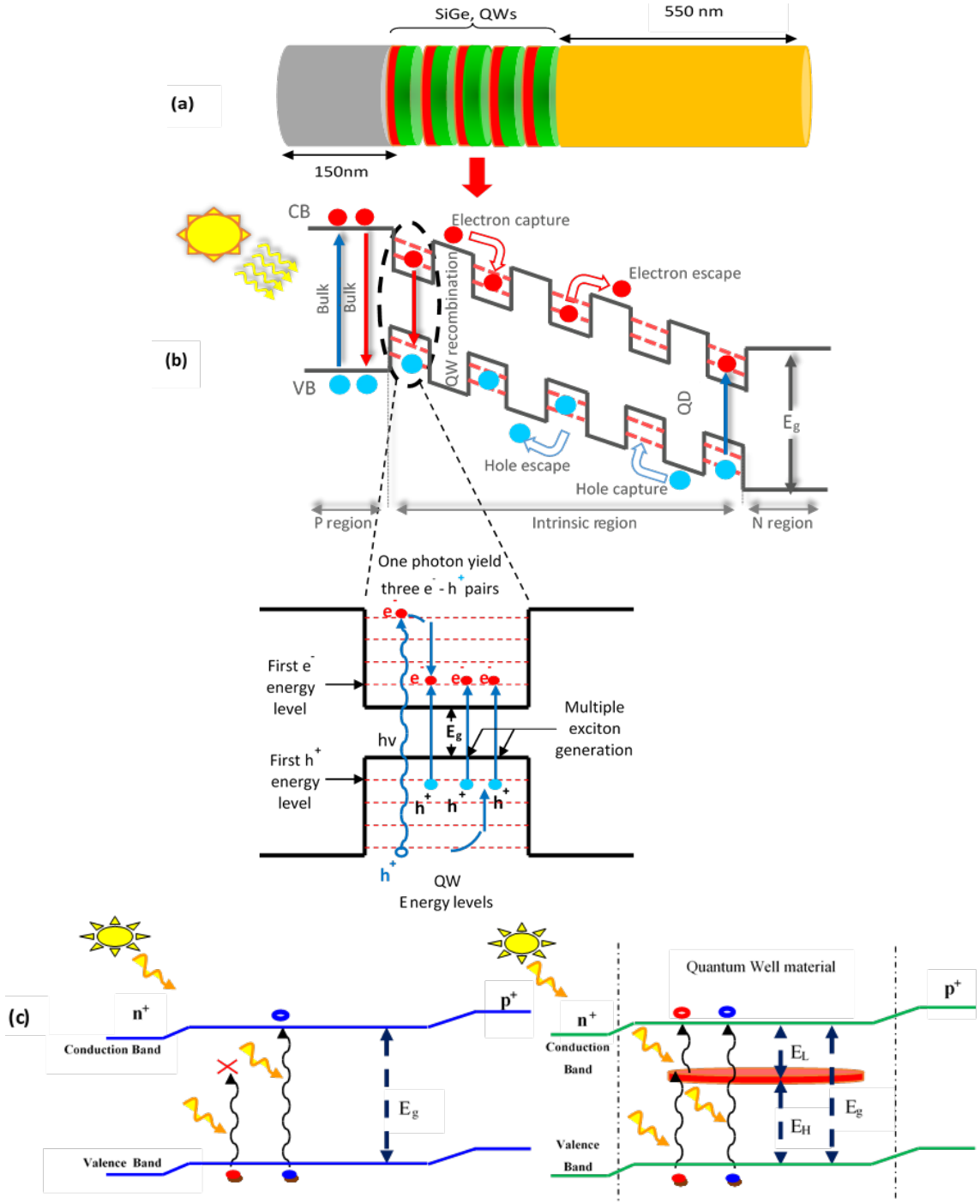

Fig. 1. Structure of a single nanowire for solar cells: (a)Single Si p-i-n nanowire, (b)Single Si p-i-n nanowire with insertion of $Si_{1-x}Ge_x$ QWs in the intrinsic region and (c)Energy band diagram of a nanowire solar cell.

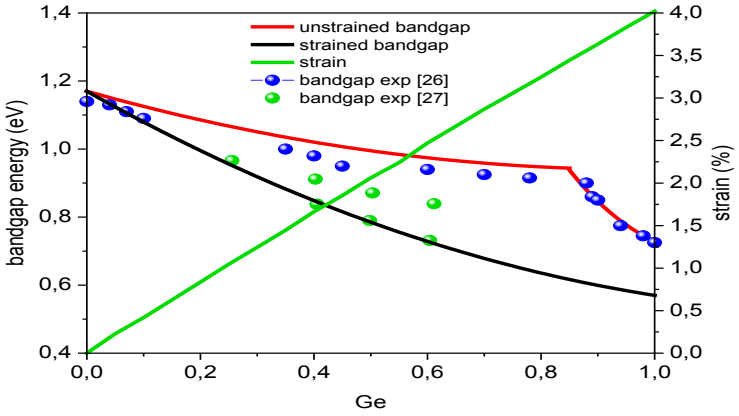

Fig. 2. Variation of bandgap energy and the strain as function of germanium concentration.

As represents the figure 3, the increase in the germanium concentration causes a decrease in the critical thickness whatever the used model. As an example, and by using Fisher model, a germanium concentration of 10 % give us an h_c equal to 4298Å, however the experimental one (bleu curve) produces h_c of 9418 Å [28], and for x=50% the critical thickness is 674 and 104 Å, so, it decreased with a value of Δh_c=3624 and 9314 Å respectively. According to this simulation, we note that the SiGe alloy can be easily grown on the Si substrate, because the critical thickness still important (above 100Å) and the epitaxial techniques allows to grow a thin layer less than 80Å [31].

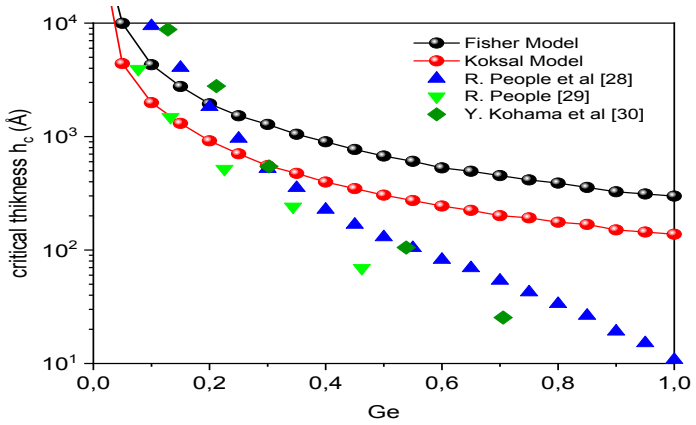

Fig. 3. Variation of the critical thickness depending on the germanium concentration.

Figure 4 shows the variation of the reflection coefficient as a function of germanium concentration. As we can see in this figure, the reflection coefficient for the unstrained and strained cases, increases with increasing germanium concentration. For example, the reflection coefficient in the strained case increases by about 0.025, while the reflection coefficient in the unstrained case increases from 0.594 to 0.613, when the germanium concentration increases from 5% to 95%. This optical parameter proves once again that the increase in concentration leads to an increase in reflection and therefore a decrease in absorption, which is unfavorable for photovoltaic applications, for this reason we focus on low concentrations. Figure 5(a) represents the energy band diagram of the solar cell including SiGe/Si QWs, for this structure we have a type II alignment, where the photocarriers are confined in the quantum well material. In this type of alignment, electrons are confined in one material (QW material), while holes are confined in the other material (barrier material). This structure allows to improve photovoltaic systems [32].

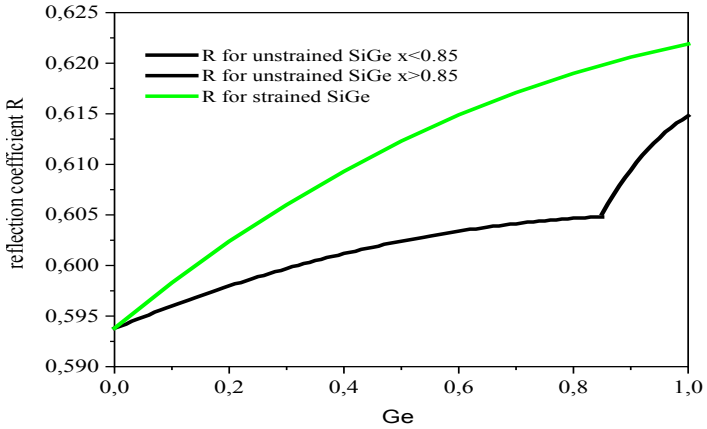

Fig. 4. Variation of the reflection coefficient as a function of germanium concentration.

Figure 5(b) illustrates the energy diagram of a single SiGe quantum well. It is clear from this figure that the band alignment is of type II and the discontinuity of the conduction band is very small by a few meV compared to the valance band [33]. This diagram allowed us to calculate the transition energies between these states for the studied structure. Figures 5(c) and 5(d) illustrate the variation of the quantization energy of the heavy holes and the transition energy as a function of the quantum well width for the two levels 1 and 2. These show that the quantization and transition energies decrease in a moderate way, where we notice that for the first level of holes, a reduction of 0.014 eV for a quantum well width varying from 10 nm to 30 nm.

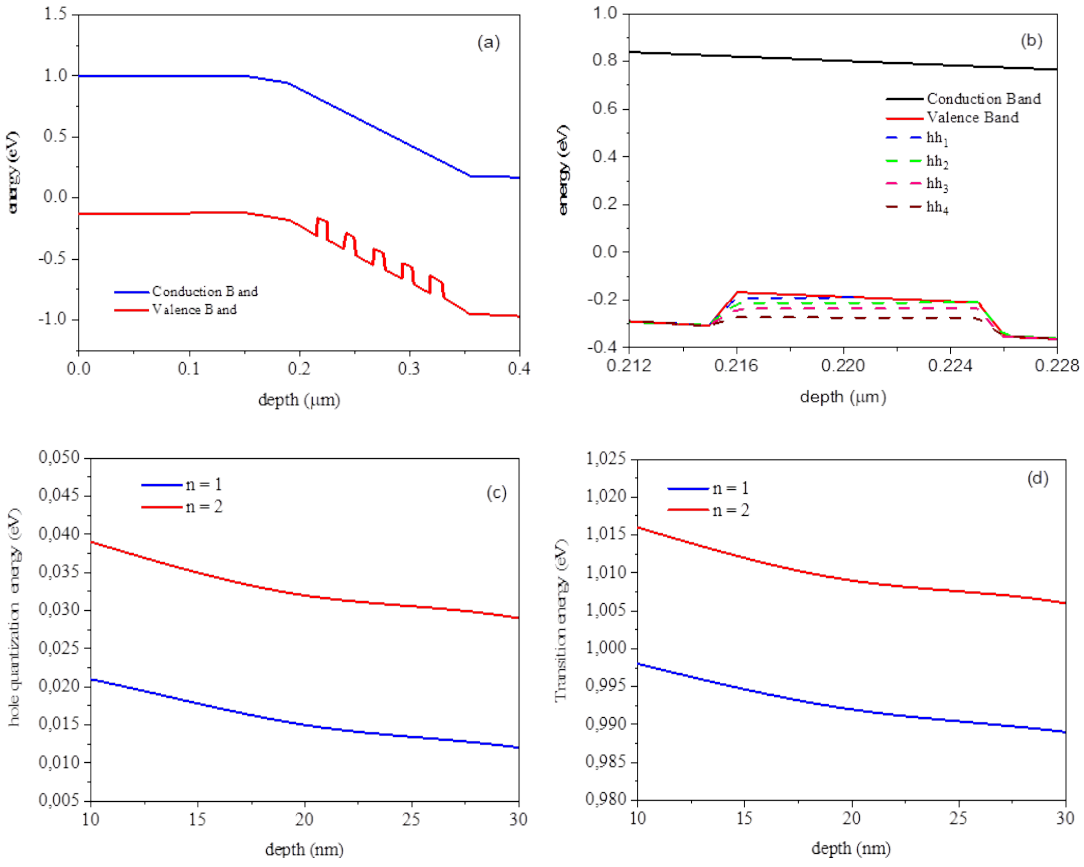

Fig. 5. Energy band diagram of a nanowires solar cell: (a) Energy band diagram of a nanowires Si with insertion of QWs SiGe/Si, (b) energy band diagram of a single SiGe quantum well (c), hole quantification energy as a function of depth and (d) transition energy as a function of depth.

We can conclude that the electronic confinement potential is more important for small QWs. This is because the latter modifies the energy states of QWs of different sizes. We also observe that the electronic confinement potential is deeper, which is related to the hydrostatic strain [34].

Figure 6 shows the spectral response as a function of wavelength for a single Si nanowire-based solar cell without QWs and with 4 QWs insertion, respectively. It was clear that the EQE of a p-i-n solar cell tends to zero at the1120 nm wavelength. It was also noticed that the spectrum broadening is extended from 1120 nm to 1200 nm compared to the p-i-n solar cell, due to the introduction of QWs. In this wavelength range, the EQE increases by 5% as the number of QW layers increases from 0 to 4; this means that photons in this wavelength range are effectively absorbed, and thus they contributed to the creation of electron-hole pairs. In addition, we have another improvement in the range of 300 to 600 nm, this improvement can be explained by the effect of the quantum wells incorporation in the intrinsic zone, this inclusion increases the width of the depletion region which in turn increases the electric field and facilitates the transport of charge carrier.

Figure 7 shows the current density characteristic (J-V) of a solar cell based on Si nanowires with insertion of 4 QWs for different germanium concentrations. As we can see, the short circuit current density (J_{sc}) decreases with increasing germanium concentration. This decrease leads to a decrease in the power delivered by the proposed structure (Fig. 8). Consequently, the difference in current density and power density of the two structures is ΔJ_{sc}=4.33 mA/cm^2 and ΔP = 1.46 mW/cm^2, respectively, comparing our structure for a 5% concentration with that of 85%. Therefore, the efficiency decreases by a factor of 5.71. Table 2 summarizes all the main characteristics of the SiGe/Si QWNW solar cell obtained in this simulation for different germanium concentrations. After this simulation, we set the germanium concentration at 5%, which gives us the best results.

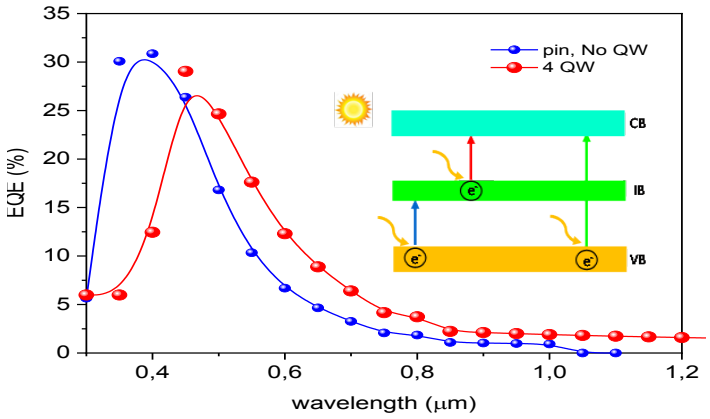

Fig. 6. External Quantum Efficiencies as a function of the wavelength for 0 and 4 quantum wells.

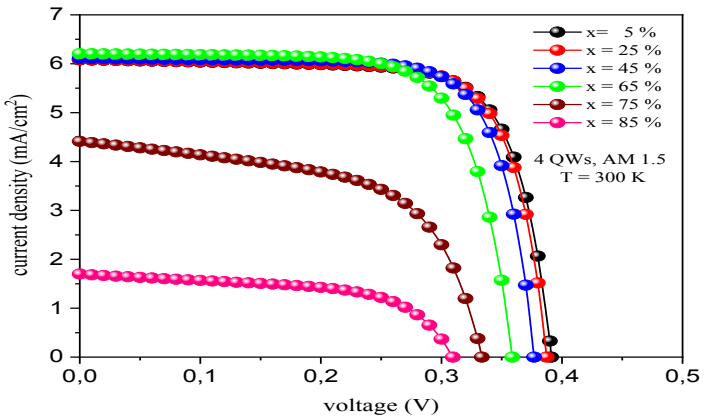

Fig. 7. J-V characteristic of a Si nanowire with insertion of 4 QWs based solar cell as a function of germanium concentration.

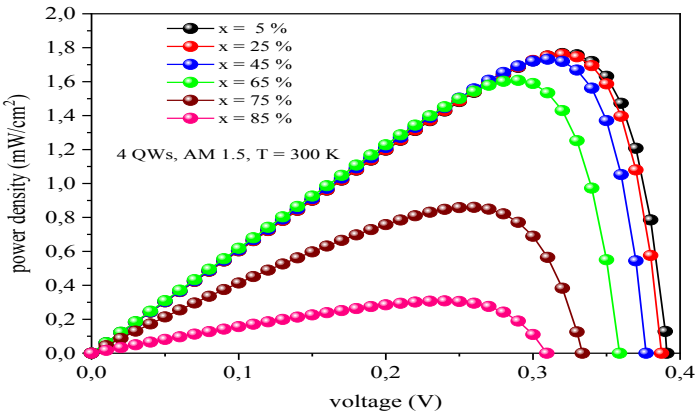

Fig. 8. P-V characteristic of a Si nanowire with insertion of 4 QWs based solar cell as a function of germanium concentration.

Table 2. Electrical characteristics of the 4 SiGe/Si QWNW for different Germanium concentration.

Ge concentration	5 %	25 %	45 %	65 %	85 %
J_{sc} *(mA/cm²)*	6,08	6,084	6,10	6,21	1,70
Voc (V)	0,391	0,39	0,38	0,36	0,31
FF (%)	74,21	74,70	75,24	72,16	58,63
η (%)	1,77	1,76	1,73	1,61	0,31

Figure 9 shows the temperature and germanium concentration effect on the conversion efficiency for 4 QWs inserted in the intrinsic region of the nanowire. As can be seen in this figure, the increase in temperature as a function of germanium concentration leads to a decrease in efficiency. There is a relative decrease of 1.87% in efficiency, when the concentration increases from 0.05 to 0.55. We can explain this decrease by the increase in the strain of the studied structure. For example, the difference in the strain of this structure is $\Delta\varepsilon$ = 6.58%, when the germanium concentration increases from x = 0.05 to x = 0.55. According to this simulation, we can once again confirm an adequate concentration value equal to 5%. Figure 10 shows the variation of the open circuit voltage (V_{oc}) and the efficiency as a function of germanium concentration, for 4 QWs inserted in the intrinsic region of the nanowire. The figure shows that increasing germanium concentration from 0.05 to 0.85 leads to a relative decrease of 17.51% in the conversion efficiency and about 8.1% in the open circuit voltage.

Figure 11 shows the evolution of the external quantum efficiency (EQE) as a function of wavelength for the three structures, Si p-i-n Nanowire, 8 QWs and 14 QWs. It can be seen that the structure with 14 QWs represents a better efficiency than that of p-i-n and 8 QWs over the entire wavelength range [0.3- 1.2] µm. For example, at a wavelength of 600 nm, the difference between the EQEs of the two structures (0 QW and 14 QWs) is ΔEQE = 6.14%. This means that the insertion of the QWs into the intrinsic region of the nanowires is useful for the solar cell in absorbing low energy photons. Also, there may be further optimization in the wavelength range from 300 nm to 450 nm. This result can be explained by the increasing number of QWs layers causing an increase in the thickness of the intrinsic region of the p-i-n solar cell. Figure 12 represents the variation of the absorption coefficient as a function of wavelength for the three Si p-i-n nanowire structures, 8 QWs and for 14 QWs inserted in the intrinsic region of the Si p-i-n nanowire. This figure confirms the importance of inserting QWs for the absorption of low energy photons, as shown in the previous figure.

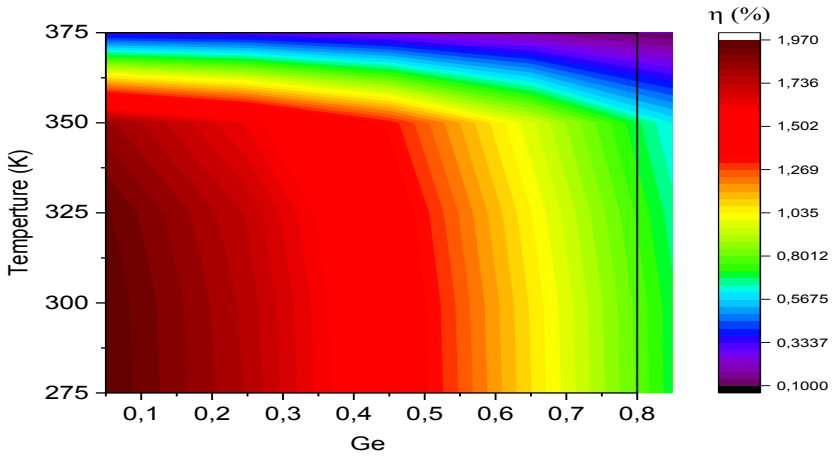

Fig. 9. Variation of the efficiency as a function of the germanium concentration and the temperature.

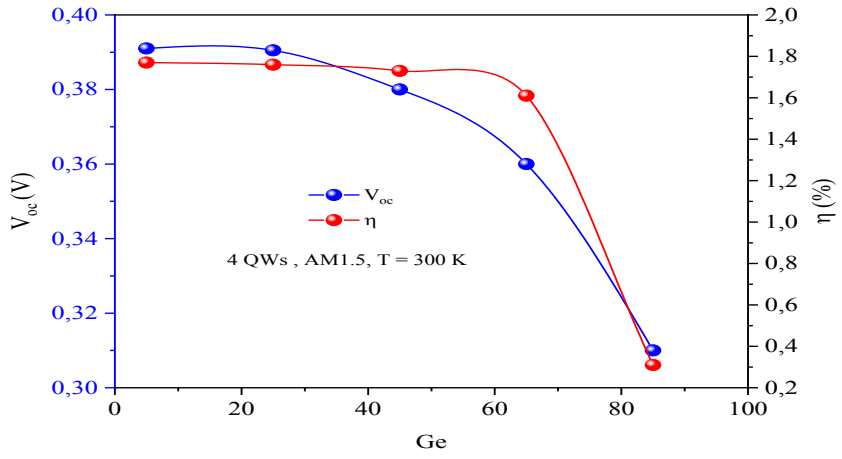

Fig. 10. Variation of the open circuit voltage and the Efficiency as a function of the germanium concentration for 4 QWs.

For this, the 14 QWs structure has a higher absorption coefficient than the p-i-n structure with 8 QWs, over the whole wavelength range. For example, the difference (between the two structures at 400 nm) is $\Delta\alpha = 1.523.10^{3}cm^{-1}$. As described above, the main purpose of inserting QWs is to absorb low energy photons, which means that these photons contribute to the creation of electron / hole pairs and ultimately to the increase of the current supplied by the cell. Figure 13 shows the J-V characteristic of a solar cell based on Si p-i-n nanowires and a $Si_{0.95}Ge_{0.05}$/Si solar cell for different number of QWs inserted in the intrinsic region. As we can see, the current density increases as the number of the inserted QWs increases.

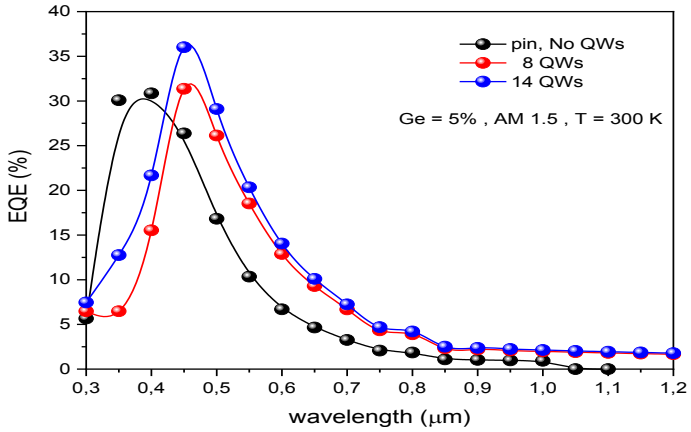

Fig. 11. Variation of EQE as a function of the wavelength for 0, 8 and 14 quantum wells.

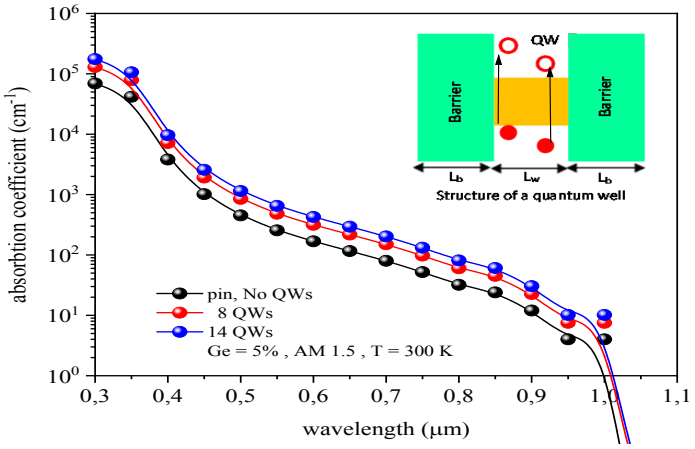

Fig. 12. Variation of the absorption coefficient as a function of the wavelength for three value of quantum wells 0, 8 and 14.

This improvement leads to an increase in the power delivered by this structure (Fig.14). Consequently, the difference in current density and power density of the two structures is ΔJ_{sc} = 1.46 mA/cm^2 and ΔP = 0.52 mW/cm^2, respectively, comparing our structure with 14 QWs with that of the Si p-i-n nanowire. Therefore, the efficiency is increased by a factor of 1.37. Table 3 summarizes all the main characteristics of the SiGe / Si QWNW solar cell obtained in this simulation for a variable number of inserted QWs. After this simulation, it has been found that the best results are given for 14 QWs, thus, we set the number of quantum wells at 14. Figure 15 exhibits the results of comparison and validation, the black and red graphs are already explained in figure 10 for Si p-i-n nanowires and the inserted QWs (14 QWs), respectively. The blue and green graphs are from two previously validated studies [35] and [36]; these graphs represent the current density of a single Si nanowire under the same conditions of our simulation.

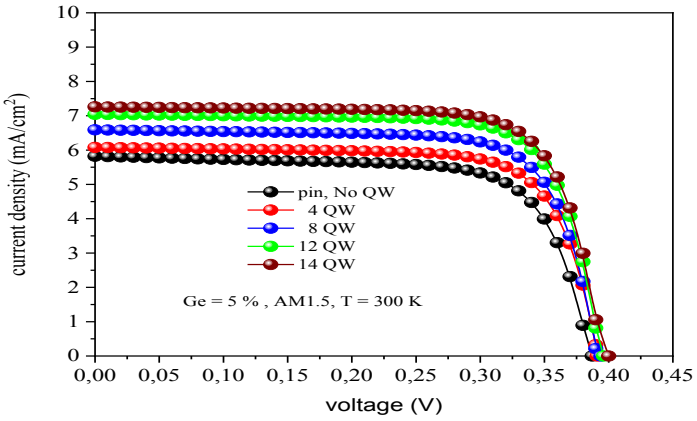

Fig. 13. J-V characteristic of a Si p-i-n nanowire based solar cell and a $Si_{0.95}Ge_{0.05}$ /Si solar cell for different number of QW inserted in the intrinsic region.

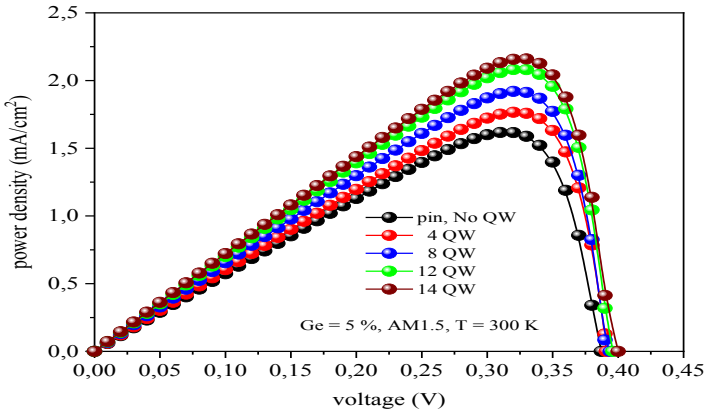

Fig. 14. P-V characteristic of a Si p-i-n nanowire based solar cell and a $Si_{0.95}Ge_{0.05}$ /Si solar cell for different number of QW inserted in the intrinsic region.

Table 3. Electrical characteristic of the SiGe/Si QWNW for different number of quantum wells.

QWs	*J_{sc}(mA/cm²)*	*V_{oc}(V)*	*FF (%)*	*η (%)*
0	5.82	0.384	72.49	1.62
4	6.08	0.391	74.21	1.77
8	6.59	0.394	76.62	1.98
12	7.04	0.396	76.76	2.14
14	7.26	0.400	76.45	2.22

We can see that our structure has a higher J_{sc} and V_{oc} compared to those of the experimental Si nanowires. A difference of ΔJ_{sc} = (simulated J_{sc} - experimental J_{sc}) is equal to 2.3 mA/cm^2 (comparing the red curve with the blue curve), and ΔJ_{sc}= 2.6 mA/cm^2 (comparing the red graph with the green graph), an improvement of the experimental J_{sc} is presented in this part. While ΔV_{oc} = (simulated V_{oc}- experimental V_{oc}) equals 0.17 V (red curve with blue curve) and ΔV_{oc}= 0.097 V (red curve with green curve). On the other hand, the structure with 14QWs presents the highest value of J_{sc} and V_{oc} compared to the simulated Si p-i-n nanowire and the experimental nanowire. This shows the interest of our study interim of efficiency. Table 3 summarizes all the main characteristics of the different structures.

In addition, as shown in figure 16, an increase in the power delivered by this structure is observed while increasing the current density, the black and red graphs are our simulated result, for both Sip-i-n nanowire and 14 QWs inserted in the intrinsic region, respectively. Also, the green and blue graphs are the power graphs from two different studies; from this figure we can observe that the proposed structure in this work has a significantly higher power than that of experimental Si nanowires with a difference of $\Delta P = 1.84$ mw/cm^2 (the difference between the red and green graphs), also $\Delta P = 1.77$mW/cm^2(the difference between the red and blue graphs). There is an obvious improvement in power between the three structures, Si 14 QWs and the two experimental structures, obviously the structure with 14 QWs remains the best.

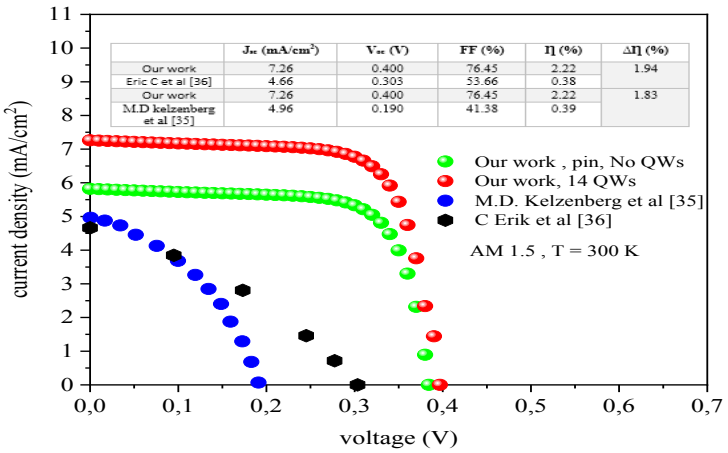

Fig. 15. J-V *comparison of our simulated structures and experimental Si nanowires.*

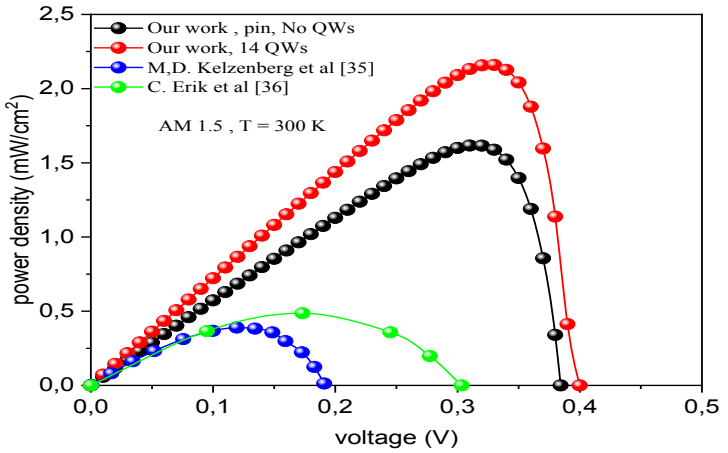

Fig. 16. P-V comparison of our simulated structures and experimental Si nanowires.

Figure 17 shows the variation of the conversion efficiency as a function of temperature and radius respectively, for 14 QWs inserted in the intrinsic region of the nanowire. As shown in this figure, on the one hand, the conversion efficiency is slightly reduced as the temperature increases, and on the other hand, it increases as the radius of the nanowire increases. For example, for a radius of 80 nm and a temperature of 275 K, the efficiency is 0.95%, and as the radius increases to 240 nm at the same temperature, the efficiency increases to 4.28%. Otherwise, for the same radius and for a temperature of 350 K, the efficiency decreases by a factor of 8.72. This decrease can be explained by the reduction of the solar cell bandgap which has an effect on the decrease of the open circuit voltage [37,38]. Figure 18 illustrates the variation of the conversion efficiency as a function of the number of integrated QWs and the radius. It can be seen that the

efficiency increases with the increase of the QWs number. This is proved by a better absorption of low energy electrons, i.e. the confinement effect. In addition, the efficiency increases with the increase of the nanowire radius

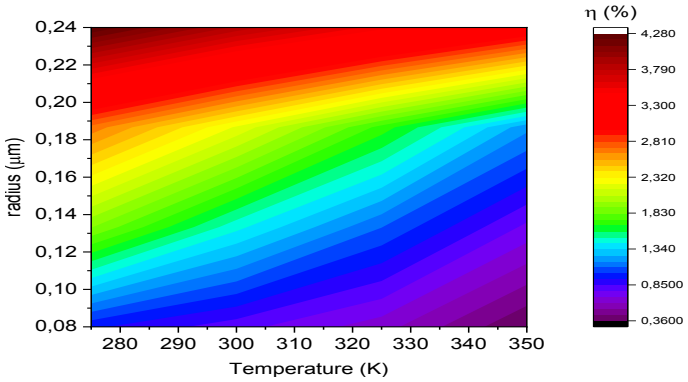

Fig. 17. Variation of the efficiency as a function of the temperature and the radius.

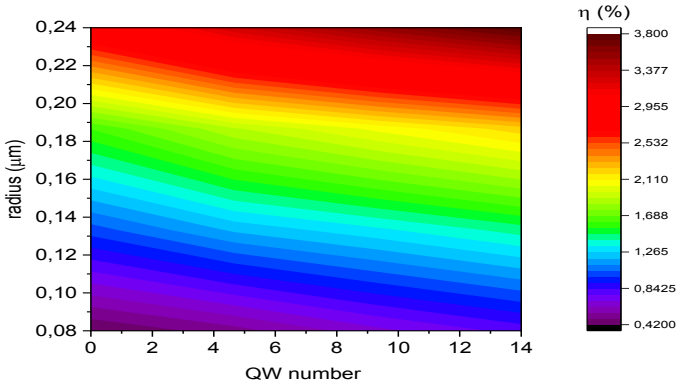

Fig. 18. Variation of the efficiency as a function of the number of wells and of rayon.

For example, the conversion efficiency increases from 0.42 to 3.80% as the radius increases from 80 nm to 240 nm and the number of the inserted QWs increases from 0 to 14. This can be explained by the increase in total area of the nanowire due to the increase in nanowire radius, which leads to better charge collection of carrier, which means better conversion efficiency. This measurement indicates that the size of a nanowire is an important issue for absorption, i.e. increasing the efficiency of the cell.

4. Conclusion

During this work, we studied the modeling of a solar cell based on silicon nanowires with insertion of SiGe quantum wells in the intrinsic part of the structure. This study sought to demonstrate the utility of well insertion in increasing solar cell efficiency. For this purpose, several characteristics were studied. First, the effect of the germanium concentration on the characteristics of the solar cell was studied; where a concentration of 5% was chosen for which the cell presents the best performances. In addition, we studied the integration of quantum wells effects on the cell performances. For this latter, the insertion of 14 QWs made of $Si_{0.95}Ge_{0,05}$ improves the cell conversion efficiency by a factor of 1.37 compared to that obtained for Si p-i-n nanowires.

Moreover, the calculation of the absorption coefficient and the EQE showed us the effect of quantum well integration for the absorption of low energy photons. As a consequence, the proposed structure with 14 $Si_{0.95}Ge_{0,05}$ QWs layers inserted in the intrinsic region, improves the efficiency by 0.6% compared to that of the Si p-i-n nanowire. Finally, the variation of temperature

and the nanowire radius was also studied and led us to optimize the conversion efficiency by a factor of 4.75, when the radius goes from 80 nm to 240 nm. This study can improve using new materials such as semiconductors III-V-(N,Sb).

References

[1] W. Shockley, H.J. Queisser, J. Appl. Phys, **32**(3), (1961)510; https://doi.org/10.1063/1.1736034
[2] E. Aouami, M. Bikerouin, M. El-Yadri, E. Feddi, F. Dujardin, M. Courel, B. Chouchen, M.H. Gazzah, H. Belmabrouk, Solar Energy journal, **201**, 339 (2020); https://doi.org/10.1016/j.solener.2020.03.011
[3] M. Piralaee, A. Asgari, Chemical Physics Letters journal, **754**, 137500 (2020); https://doi.org/10.1016/j.cplett.2020.137500
[4] Y. Wang, Y. Zhang, D. Zhang, S. He and X. Li, Nanoscale Research Letters, **10**(1) , 1 (2015); https://doi.org/10.1186/s11671-015-0968-2
[5] A. Chowdhury, M. Trudeau, R. Wang, H. Guo, Z. Mi, Appl. Phys. Lett, **118**(1), 012101 (2021); https://doi.org/10.1063/5.0029761
[6] V.I. Klimov, J. Phys. Chem, **110**(34), 16827 (2006); https://doi.org/10.1021/jp0615959
[7] A.J. Nozik, Nano Lett, 10(8), 2735 (2010); https://doi.org/10.1021/nl102122x
[8] N. N. Greenwood, A.Earnshaw, "Chemistry of the Elements 2nd Edition", Butterworth-Heinemann, 328 (1997); ISBN-13. 978-0750633659
[9] A. Aissat, F. Benyettou, J. P. Vilcot, Modélisation et simulation des cellules solaires à puits quantique à base de SiGe/Si,International Journal of Hydrogen Energy, 10, 1 (2016).
[10] P. Ashburn, D. M. Bagnall, "silicon-Germanium : Properties, growth and Applications", Springer Handbook of Electronic and Photonic Materials, 481 (2006); https://doi.org/10.1007/978-3-319-48933-9_22
[11] Y. Li, G.Wang, M. Akbari-Saatlu, M.Procek and H. H. Radamson, Frontiers in Materials, **8**, 611078 (2021); https://doi.org/10.3389/fmats.2021.611078
[12] M.Safi, A.Aissat , H.Guesmi, I.Barbezier, Modeling of Si-Based Nanowires by Insertion of SiGe Quantum Wells (QWNW). 6th International Renewable and Sustainable Energy Conference (IRSEC) (pp. 1-4), (2018) IEEE; DOI: 10.1109/IRSEC.2018.8702282
[13] L. Fonseca, I. Donmez-Noyan, M. Dolcet, D. Estrada-Wiese, J. Santander, M. Salleras, A. Tarancon , Nanomaterials journal, **11**(2), 517 (2021) ; https://doi.org/10.3390/nano11020517
[14] X. Shi, J. Zou, Z. Chen, Advanced Thermoelectric Design: From Materials and Structures to Devices, chemical reviews, **120**(15), 7399 (2020); https://doi.org/10.1021/acs.chemrev.0c00026
[15] Y. M. Haddara, P. Ashburn, D. M. Bagnall, " Silicon-Germanium: Properties, Growth and Applications. In: Kasap, S., Capper, P", Springer Handbook of Electronic and Photonic Materials. Springer Handbooks. Springer. Cham, (2017); https://doi.org/10.1007/978-3-319-48933-9_22
[16] K. Koksal, B. Gonul, and Oduncuoglu, The European Physical Journal B, **69**, 211 (2009); https://doi.org/10.1140/epjb/e2009-00151-2
[17] S. Almosi, C. Robert, T. Nguyen Thanh, C. Cornet, A. Létoublon et al, Journal of Applied Physics, **113**, 123509(2013); https://doi.org/10.1063/1.4798363
[18] A. Fischer, H. Kuhne, and H. Richter, Phys. Rev. Lett, **73**(20), 2712 (1994); https://doi.org/10.1103/PhysRevLett.73.2712
[19] R. Khoie, S. M. Ramey, Physica E, **34**(1-2), 449 (2006) ; https://doi.org/10.1016/j.physe.2006.03.133
[20] D. Munteanu, J. L. Autran, "A 2-D/3-Dchrödinger-Poisson Drift-Diffusion Numerical Simulation of Radially-Symmetric Nanowire MOSFETs, Nanowires - Recent Advances" , IntechOpen, 341 (2012); ISBN 978-953-51-0898-6
[21] C. I. Cabrera, J. C. Rimada, L. Hernández, D. A. Contreras-Solorio, Superf. vacío , **25**(4), 234 (2012).
[22] J. Geist, A. R. Schaefer, J. F. Song, Y. H. Wang, E. F. Zalewski, Journal of research of the National Institute of Standards and Technology, **95**(5), 549 (1990); doi: 10.6028/jres.095.043

[23] G .Lasher, F. Stern, Phys Rev, **133**(2A), 553 (1964); https://doi.org/10.1103/PhysRev.133.A553
[24] M. Seifikar, E. P. O'Reilly, S. Fahy, Nanoscale Res Lett, **9**(1), 51 (2014); https://doi.org/10.1186/1556-276X-9-51
[25] A. El Aouami,· E. Feddi,· A. Talbi,· F. Dujardin, C. A. Duque, Appl. Phys. A, **124**(6), 442 (2018) ; https://doi.org/10.1007/s00339-018-1856-2
[26] R. Braunstein, A. R. Moore, and F. Herman, Phys. Rev, **109**(3), 695 (1958); https://doi.org/10.1103/PhysRev.109.695
[27] D. V. Lang, R. People, J. C. Bean, and A. M. Sergent, Appl. Phys, Lett. **47**(12), 1333 (1985); https://doi.org/10.1063/1.96271
[28] R. People and J. Bean, Applied Physics Letters, **49**(4), 229 (1986); https://doi.org/10.1063/1.97637
[29] R. People, IEEE Journal of Quantum Electronics, **22**(9), 1696 (1986); DOI: 10.1109/JQE.1986.1073152
[30] Y. Kohama, Y. Fukuda and M. Seki , Appl. Phys, Lett, **52**(5), 380 (1988); https://doi.org/10.1063/1.99472
[31] T. Soga, "Nanostructured Materials for Solar Energy Conversion", Elsevier Science (2006).
[32] D. Rekioua, E. Matagne, "Optimization of Photovoltaic Power Systems: Modelization, Simulation and Control", Green Energy and Technology, 284 (2012) .
[33] R. People, J. C. Bean, O. V. Lang, A. M. Sergent, H. L. Stormer, K. W. Wecht, R. T. Lynch, and K. Baldwin, Appl. Phys. Lett, **45**(11), 1231 (1984); https://doi.org/10.1063/1.95074
[34] A .Faraji, S. Sabri, R. Malek, K. Kassmi, Materials Today: Proceedings, **45**, 7329 (2021); https://doi.org/10.1016/j.matpr.2021.01.001
[35] M.D. Kelzenberg, B. Turner-Evans, M. Kayes, A. Filler, C. Putnam, S. Lewis, H.A. Atwater, Nano Letters, **8**(2), 710 (2008); https://doi.org/10.1021/nl072622p
[36] K. Q. Peng, S. T. Lee, Adv. Mater, **23**(2), 198 (2011); https://doi.org/10.1002/adma.201002410
[37] P. Singh, S. N. Singh, M. Lal, M. Husain, Solar Energy Materials and Solar Cells, **92**(12), 1611 (2008); https://doi.org/10.1016/j.solmat.2008.07.010
[38] P. Singh, N. M. Ravindra, Solar Energy Materials and Solar Cells, **101**, 36 (2012); https://doi.org/10.1016/j.solmat.2012.02.019